NANO: Brief Reports and Reviews
Vol. 7, No. 1 (2012) 1150003 (9 pages)

DOI: 10.1142/S1793292011500032

World Scientific
www.worldscientific.com

ELASTIC SURFACE PLASMON POLARITON SCATTERING: NEAR- AND FAR-FIELD INTERACTIONS

PAULINA SEGOVIA
Universidad Autonoma de Nuevo Leon
Doctorado en Inegnieria Fisica Industiral-FCFM, Pedro de Alba S/N
San Nicolas de los Garza, Nuevo Leon, 66451, Mexico
psegovia@cicese.mx

VICTOR COELLO
Centro de Investigación Científica y de Estudios
Superiores de Ensenada BC, Unidad Monterrey
Km 9.5 Carretera Aeropuerto, Parque de Investigacion e
Innovacion Tecnologica (PIIT) Apodaca
Nuevo Leon, 66629, Mexico
vcoello@cicese.mx

Received 22 September 2011
Accepted 9 November 2011
Published 23 February 2012

Using a vectorial dipolar model for multiple surface plasmon-polariton (SPP) scattering, we investigate propagation and elastic (in-plane) scattering of SPP's excited in the wavelength range of 543−633 nm at random nanostructured gold surfaces. The model makes use of a composed analytic Green dyadic which takes into account near- and far-field regions, with the latter being approximated by the part describing the scattering via excitation of SPP. Simultaneous SPP excitation and in-plane propagation inside square-random arrays of nanoparticles were observed with different density of particles, demonstrating the feasibility of the suggested approach. The composed Green dyadic represents an improvement of previous SPP simulations for random nanoparticles arrays since it permits SPP scattering simulations for more realistic systems with relatively large number of close, or even in contact, nanoparticles. Our results suggest that this numerical approach is quite promising for the quantitative description of light-SPP coupling and associated processes such as weak and strong SPP localization.

Keywords: Surface plasmon polaritons; green dyadic; multiple scattering.

1. Introduction

Surface plasmon polaritons (SPPs) are oscillations of surface electron charge density which can exist at a metal/dielectric interface.[1,2] Associated with them, there is an electromagnetic field propagating along the interface with exponential decays perpendicular to it. For this reason, SPPs exhibit an extremely high sensitivity to surface properties

such as roughness and surface adsorbates.[1,2] Due to their electromagnetic nature, SPP can diffract, reflect and interfere. These properties are clearly exhibited in the course of SPP scattering.[3] Scattering of SPPs is usually caused by randomly placed surface imperfections since even the most carefully prepared surfaces are not completely flat. Such scattering process comprehends either elastic scattering i.e., in the surface plane, giving rise to a diverging cylindrical SPP, or inelastic scattering i.e., field components propagating away from the surface. In general, both elastic and inelastic scattering processes result in decreasing the efficiency of SPP excitation, which also depends on the film thickness and dielectric constant.[1,2] Concerning SPP excitation by light, conventionally most of SPP excitations methods are based on the use of glass prisms as couplers.[1,2] Those methods have some drawbacks such as the large size of the prism couplers that make them not suitable for photonic integrated circuits. As an alternative one can make use of normal incident light in order to excite the SPP through a ridge or subwavelength-hole arrays located at the top of an air/metal interface. Such SPP launching mechanisms have been used for quantitative experimental analysis of a SPP interferometer,[4] nanoparabolic chains,[5] and testing of refractive plasmonic structures based on nanoparticles.[6] Considering the SPP interaction with and manipulation by arrays of surface nanoparticles,[4–17] extensive theoretical studies have been conducted. The problem is not trivial since even a simple case, as a single symmetric nanoparticle, requires elaborated numerical calculations.[18] In this context, the point-dipole approximation has shown to be an accurate and relative simple method for calculation of elastic SPP scattering.[3] The point-dipole model has been used, for simulation of SPP microcomponents[3] and photonic band-gap structures[19] formed by a set of dipolar nanoparticles. On the other hand, using the same approach, a theory for light scattering from a random array of nanoparticles, spaced much less than an optical wavelength was developed.[20] The scalar model of Ref. 3 was extended into a vectorial dipolar model for SPP multiple scattering[21] and used to calculate SPP scattering produced by band-gap structures and model the operation of a micro-optical SPP interferometer.[22] Here, certain limitations on the accuracy of numerical results should be borne in mind. For example, the effective polarizability in Ref. 3 of an individual particle is a phenomenological quantity that is difficult to relate to particle parameters such as size, susceptibility, etc. It is interesting to notice, however, that the size of the scatterer, which would correspond to the effective polarizability used in Ref. 3, seems reasonable and sufficiently small with respect to the wavelength, so that, in that case, the point-dipole approach can still be considered adequate for the modeling of SPP scattering phenomena. In general the dipole model allows one to avoid, up to some extent, the complicated mathematical treatment involved in the problem of SPP scattering by surface inhomogeneities. However, one should take into account that the point-dipole approximation for SPP scattering has not been fully explored, and the limits of its validity have not yet completely established.[23] For example in the case of randomly placed nanoparticles with relatively high densities, some particles are in or close to contact with each other so that the interparticles distances can be down to a small fraction of the wavelength, i.e., in the near-field domain.[24] The main purpose of this paper is to consider the use of near- and far-field terms in the modeling of elastic scattering of SPP-fields along a surface. The model exploits the analytic representations of the Green dyadic in the near- and far-field regions, with the latter being approximated by the part describing the scattering via SPP excitation. In general, one of the serious problems in the local imaging of SPPs fields[25] is related to the fact that the resulting intensity images are complicated and difficult to interpret in a clear way. The SPP numerical modeling here proposed can represent an improvement in the understanding of plasmonic phenomena for periodic[5,6] or random[26–30] nanoparticles arrays as well as for systems of relatively close nanoparticles.

2. The Model

The numerical model is based on the following assumptions: (i) The elastic SPP scattering is dominant with respect to the inelastic SPP scattering and (ii) when light is incident on a metal/dielectric interface with scattering objects, the objects can be modeled as point-like dipoles (Fig. 1).

These assumptions lead to the construction of an approximate Green's tensor describing the near- and far-field terms produced by such dipoles. Thus, the self-consistent field at the site of the scatterers

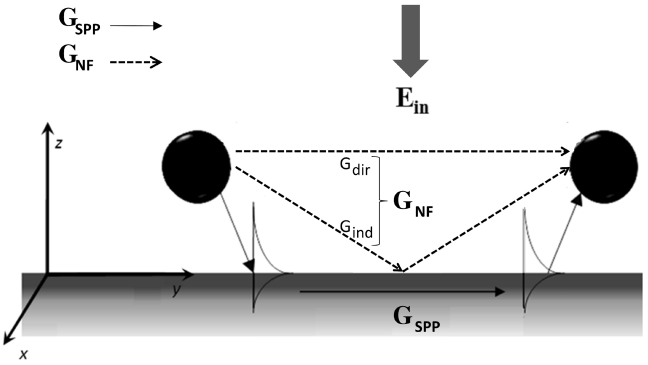

Fig. 1. Schematic representation of the near- and far-field Green dyadics. The use of one or another primarily will depend on the interparticle distances. SPP to SPP interaction is pictorially represented as solid arrow. The Near-Field Dyadic has two contributions which are: Direct and Indirect components are pictorially represented with three arrows.

in the process of multiple scattering takes the form:

$$E(r_j) = E_0(r_i) + k_0^2 \sum_{j \neq i}^{N} G(r_i, r_j) \cdot \alpha \cdot E(r_j)\,, \quad (1)$$

where $E_0(r_i)$ is the self-consistent field at the site of scatterer i, k_0 is the wave vector of the incoming field in the space, $G(r_i, r_j)$ is the Green tensor for near- and far-field regions (total field propagator), α is the polarizability of the scatterers. Here the polarizability α has the surface dressing included i.e., the coupling of the dipole to itself through reflection in the surface. Futhermore, the polarizability, α, is a tensor, describing the polarizability effect in each direction[20]:

$$\alpha = \left(I - k_0^2 \frac{\alpha^0}{\varepsilon_0} \cdot G^S(r, r') \right)^{-1} \cdot \alpha^0\,, \quad (2)$$

where α^0 is the free space polarizability tensor given as

$$\alpha^0 = \varepsilon_0 I 4\pi a^3 \frac{\varepsilon - 1}{\varepsilon + 2}, \quad (3)$$

with I being the unit dyadic tensor, ε is the dielectric function (wavelength dependent), a is its radius and ε_0 is the vacuum permitivity. Equation (2) is valid when the long-wavelength electrostastic approximation has been used. Such approximation assumes that the field is constant within the considered range, which corresponds to the size of the scatterer. For the approximation to be valid, the wavelength must be much bigger than the size of the scatterer. If the image dipole approximation is used on $G^S(r, r')$ in Eq. (2) the following result is obtained for the polarizability tensor of Eq. (1):

$$\alpha \approx \left[\frac{\varepsilon - 1}{\varepsilon + 1} \cdot \frac{\varepsilon - 1}{\varepsilon + 2} \left(\frac{1}{8} \hat{x}\hat{x} + \frac{1}{8} \hat{y}\hat{y} + \frac{1}{4} \hat{z}\hat{z} \right) \right]^{-1} \cdot \alpha^0\,. \quad (4)$$

It should be mentioned that the dipole approximation assumes that the phase delay of the field, when it moves over the scatterer, is negligible. Mathematically this means $e^{k \cdot r} \cong 1$ for a given field. This means again that the size of the scatterer should be smaller than the wavelength, which is the main assumption in the model. When Eq. (4) has been used in Eq. (1) to determine the polarization, the final step is to calculate the field outside the scatterer as a self-consistent field:

$$E(r) = E^0(r) + k_0^2 \sum_{i}^{N} G(r, r_i) \cdot \alpha \cdot E(r_i)\,. \quad (5)$$

The Green tensor for SPP to SPP scattering (far-field) is the sum of a direct contribution, G^d, in this case the free space Green's tensor, and an indirect contribution, G^S, that describes both reflection from the metal/dielectric interface and excitation of SPPs. Considering both the source and observation points being close to a metal surface but far away from each other, one can propose to use a three-dimensional dyadic Green's tensor approximation which accounts only for the SPP elastic scattering channel and which includes the direct and indirect terms with the part of the indirect Green dyadic concerned with the excitation of SPPs. Therefore, the Green dyadic can be represented by:

$$G_{\mathrm{SPP}}(rr') \approx a_{zz}(\lambda) \exp[i\kappa_z(z+h)] H_0^1(\kappa_\rho \rho) \times \left[\hat{z}\hat{z} + (\hat{z}\hat{\rho} - \hat{\rho}\hat{z}) \frac{\kappa_z}{\kappa_\rho} - \hat{\rho}\hat{\rho} \left(\frac{\kappa_z}{\kappa_\rho} \right)^2 \right], \quad (6)$$

where H_0^1 is the zero-order Hankel function of the first kind, $\rho = |r_\parallel - r'_\parallel|$, $\hat{\rho} = (r_\parallel - r'_\parallel)/\rho$, with $\parallel$ referring to the projection of the radius vector on the xy plane which coincides with the metal/air interface, and z refers to the height of the observation point r above the surface, while h refers to the height of the source point r'. Finally, κ_ρ and κ_z are the components of the three-dimensional SPP wave vector

$$\kappa_\rho = k_0 \sqrt{\frac{\varepsilon}{\varepsilon + 1}}, \quad \kappa_z = \sqrt{k_0^2 - \kappa_\rho^2}\,, \quad (7)$$

and

$$a_{zz}(\lambda) = \frac{\kappa_\rho}{2}\left[\sqrt{\varepsilon}\left(1-\frac{1}{\varepsilon^2}\right)\frac{1+\varepsilon}{\varepsilon}\right]^{-1}. \quad (8)$$

The Green dyadic above described has proven effective in analyzing plasmonics phenomena in a variety of contexts.[17] Such approximation is a far-field approximation in the sense that the corresponding field satisfies the Maxwell equations only at sufficiently large distances from a source, i.e., in the far-field zone ($\sim > \lambda/2$). In principle, it can be corrected by adding more terms in such a way that the generated field would be physical also at small distances ($\sim < \lambda/2$). Thus, special attention needs to be paid to the multiple scattering in systems with a high density of particles where such particles are very close or even in physical contact with each other i.e., in the near-field domain. In such a case, one should take advantage of the near-field electrostatic approximation of the total Green dyadic:

$$G_{\rm nf}(r, r_s, \omega) = D_{\rm nf}(r, r_s, \omega) + I_{\rm nf}(r, r_s, \omega), \quad (9)$$

where $D_{\rm nf}(r, r_s, \omega)$ is the direct part of the near-field propagator given by

$$D_{\rm nf}(r, r_s, \omega) = -\frac{c^2}{4\pi\omega^2}\frac{3e_R e_R - U}{R^3}, \quad (10)$$

with r_s being the source point, $R = |r - r_s|$, $e_R = (r - r_s)/R$, ω is the incident light frequency, and U being the unit tensor.

The indirect propagator, $I_{\rm nf}(r, r_s, \omega)$ has a complicated form and is usually expressed via its FT.[31] However, in the nonretarded and local limit of the bulk response, the dipole−dipole interaction can be treated as a direct interaction between the dipole and its mirror image.[32,33] Thus, if the bulk surface coincides with the plane $z = 0$, $I_{\rm nf}(r, r_s, \omega)$ can be expressed in the flowing form:

$$I_{\rm nf}(r, r_s, \omega) = D_{\rm nf}(r, r_{\rm ms}, \omega) \cdot M(\omega), \quad (11)$$

where $r_{\rm ms}$ points to the position of the mirror image of the source and

$$M(\omega) = \frac{\varepsilon - 1}{\varepsilon + 1}\begin{pmatrix} -1 & 0 & 0 \\ 0 & -1 & 0 \\ 0 & 0 & 1 \end{pmatrix}. \quad (12)$$

Both approximations considered above are then limited to either short or long interaction distances. The main idea of our approach is to use the near-field dyadic for distances shorter and the SPP dyadic for distances longer, than a certain transition distance related to a specified fraction of the light wavelength used in the particular simulations. Bearing that in mind, we proceed to calculate such a transition.

A natural requirement to such a transition distance would then be that no apparent unphysical jumps should be seen in the dyadic components when switching from one expression to another one. In order to find a proper distance for the transition between the two dyadics, the radial dependence of the nonzero dyadic components Gzz, Gxx and $Gzx = Gxz$ were calculated using accordingly Eqs. (6) and (9) at different distances from the gold surface and for different transition distances at the wavelengths of 633 nm, 604 nm, 594 nm and 543 nm. In Figs. 2(a)−2(d) the left side of the vertical dashed line corresponds to the Green near-field dyadic components whereas the right side, of the same line, corresponds to the SPP Green dyadic components. Based on these calculations the transition distance of $3\,\lambda/5$ was chosen [Figs. 2(a)−2(d)]. In general, it is not possible to find the transition distance that would ensure smooth transitions for all dyadic components. However, the aim is to keep a relatively simple approach and use it in a complex surface system i.e., with many strongly interacting particles.

3. Numerical Results

When considering periodic nanoparticles arrays with interparticle distances smaller than the excitation wavelength yet significantly larger than the sizes of nanoparticles, their behavior in an optical potential is well described by the vectorial dipolar model for multiple SPP scattering.[21] On the other hand, when the interparticle distance is of about a small fraction of the wavelength, i.e., in the near-field domain, more complicated behaviors are to be expected especially in nanoparticles systems with relatively high densities and a transition distance for the dyadic components [Figs. 2(a)−2(d)] should be considered. Following a step-by-step process, first we examine and compare resulting scattering processes between the two approximation methods above mentioned. We calculate the in-plane scattered field created by a normally incident Gaussian beam ($\lambda_0 = 633$ nm, FWHM $= 4\,\mu$m, y-pol) of unit amplitude impinging on a 125-nm-period square lattice (width $w \approx 0.8\,\mu$m, length $L \approx 12.5\,\mu$m) of

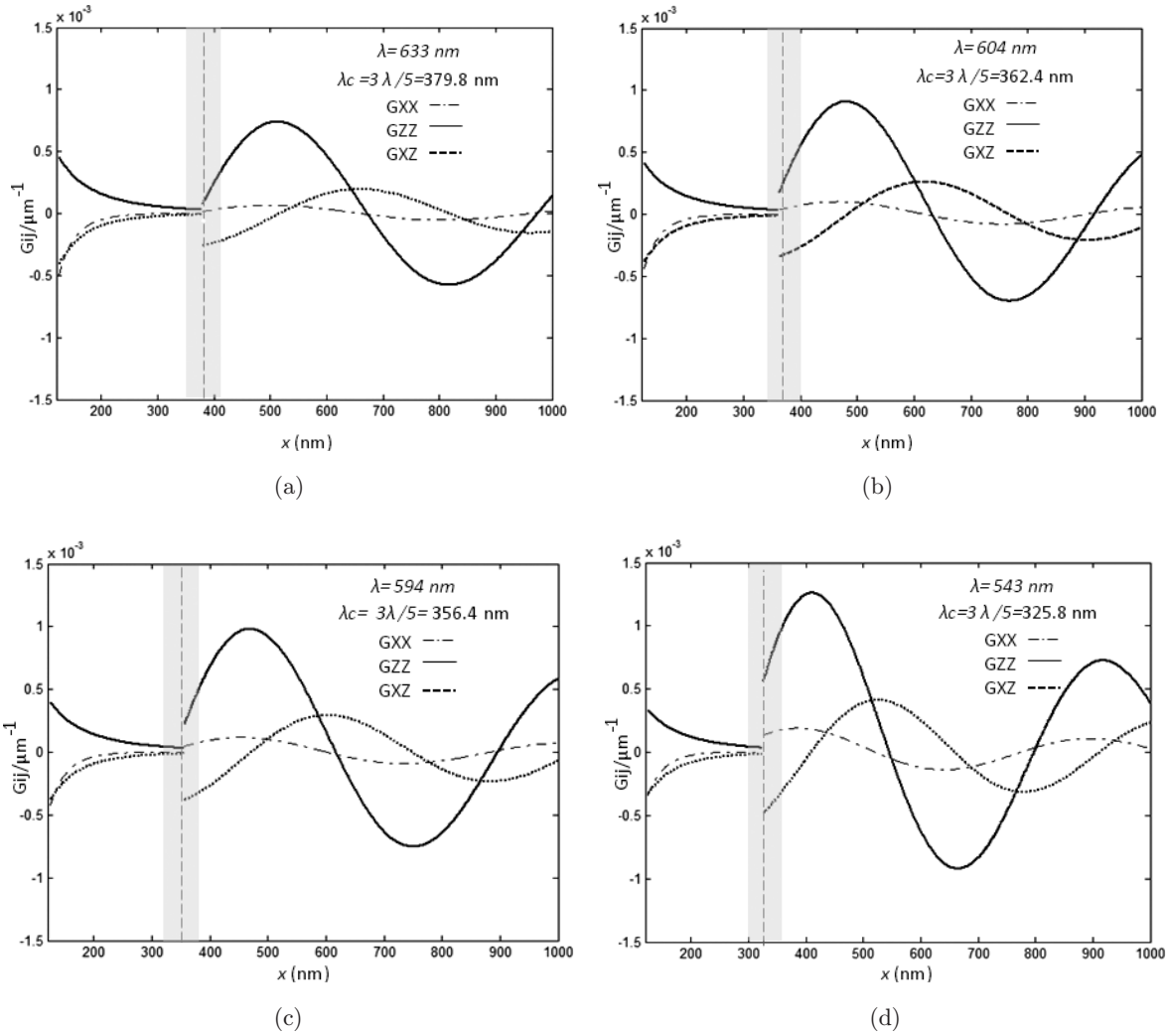

Fig. 2. Nonzero dyadic components calculated for different wavelengths: (a) 633 nm, (b) 604 nm, (c) 594 nm and (d) 543 nm using the near-field and SPP dyadic for distances correspondingly smaller and larger than the value of $3\lambda/5$ which is centered in a transition zone of 30 nm (gray areas). Axis x has the same orientation as in Fig. 1.

nanoparticles with radius, r, of 20 nm [Figs. 3(a) and 3(b)].

The entire system is simulated on a gold surface with dielectric constant $\varepsilon = -9.5093 + 1.21i$. Hereafter, for all images, that value is used, the total field is calculated 80 nm above the air−gold interface, and the incident beam has been removed. Such configuration and the illumination conditions, in general, can be considered as fairly similar to experimental realized ones.[5,6] Figures 3(a) and 3(b) show numerical simulations of a direct SPP excitation taking place at the lower (along y-axis) nanoarray edge likewise propagating SPP modes are excited in thin-film surface utilizing gratings or ridges. The results show almost no differences, for this particular geometry, between the two approaches. At the excitation nanoarray edge, the number of particles that are in contact over the extent of the incident beam is relatively low and therefore the multiple scattering is dominated by the Green dyadic concerned with the excitation of SPPs rather than by relatively near-field local interactions. A similar effect can be obtained when considering a normally incident Gaussian beam impinging on a randomly distributed system of relative low (60) number of particles [Figs. 4(a)−4(c)].

There, we can observe that the total intensity distributions [Figs. 4(b) and 4(c)] are the same besides that the image in Fig. 4(c) is brightened by a few bright-spots. In contrast, significant difference is observed, in the overall behavior of the total intensity distributions, when the images are

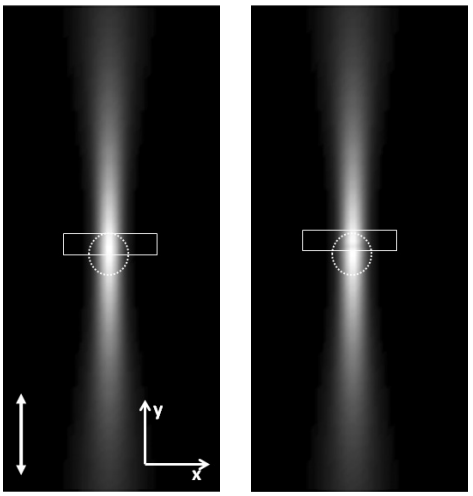

(a) (b)

Fig. 3. Electric field magnitude distributions ($100 \times 30\,\mu m^2$) calculated considering only the far-field propagator (a) and using the composed Green dyalic (b). The dotted circle represents the incident Gaussian beam (wavelength, $\lambda = 633\,nm$, FWHM $= 4\,\mu m$, y-pol) being incident on the nanoarray (white rectangular). The white arrow in (a) indicates the incident light polarization in both cases.

calculated using a dense scattering region of 300 particles [Figs. 5(a)–5(c)].

In general, in both images [Figs. 5(b) and 5(c)], one can appreciate bright and dark regions which are a collection of small and round bright spots similar to those reported as evidence of localized SPPs.[34]

However, in the SPP Green dyadic approximation [Fig. 5(b)], one can observe that even though the numerical analysis was performed under the assumption of multiple scattering behavior, the resulting interference pattern was not quite complicated as one would generally expect in a high-density nanoarray of particles. This is a major issue especially in SPP localization modeling where, in order to optimize the effect, a large volume of nanoparticles is needed.[34] In this context the composed Green dyadic may be the most appropriate approach. Consideration of the appropriate Green dyadic can lead to a better understanding of the SPP scattering effects. Concerning random scatterers, the light wavelength influence on the intensity distributions in the multiple scattering regime (inside of the scatterer area) was another aspect to be considered. The wavelength dependence is a feature inherent to the phenomenon of multiple scattering. Using the composed Green dyadic, we calculate the total intensity distribution, for different illumination wavelengths, in a nanoparticle array similar to the array shown in Figs. 6(a)–6(e).

There, we could observe clear differences in the interference patterns calculated. In particular, these changes can be observed in the exchange of positions of the bright zones appearing on the calculated intensity distributions.

Another line to check the capability and accuracy of our current numerical model is related to the statistics of the optical signal enhancement[35,36] in the corresponding images. In general the phenomena related to the regime of coherent multiple light scattering are rather complicated and their interpretation is far from being trivial. With multiple scattering, the randomness of the interactions yields a large number of scattering events. Furthermore, two images with the same number of

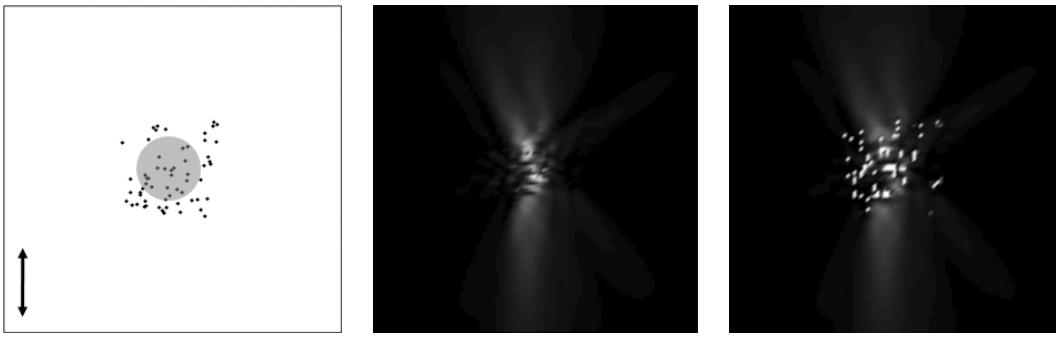

(a) (b) (c)

Fig. 4. Electric field magnitude distributions ($10 \times 10\,\mu m^2$) for an array of low number of scatters (a) calculated considering only the far-field propagator (b) and using the composed Green dyadic (c) at a wavelength of 633 nm. The gray circle in (a) represents the incident Gaussian beam with the polarization configuration indicated by arrow.

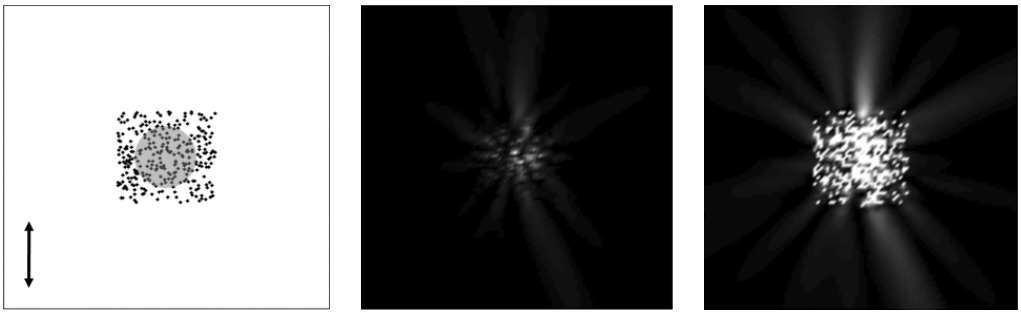

(a) (b) (c)

Fig. 5. Electric field magnitude distributions ($10 \times 10\,\mu m^2$) calculated for an array of a high number of scatters (a) obtained with SPP propagator (b) and considering the near-field propagator (c) at a wavelength of 633 nm. Incident Gaussian beam and its polarizations are represented as in Fig. 4.

particles but different distributions exhibit distinct total intensity fields. Indeed, a small variation of the particles distributions and/or parameters of the incident light may change significantly the total intensity field distribution. This feature makes the comparison of different scattering configurations complicated, especially because bright spots can be quite different even for the same nanoparticle distribution (Fig. 6). In this context, it was demonstrated that a probability density function (PDF) exhibits a significant statistical difference for total field intensity distributions established in different scattering regimes, viz., weak and strong SPP scattering.[34] Here, the basis of our probability sampling was the selection of sampling units from the images that were calculated using the same excitation wavelength and light polarization (y-pol). The average value of the calculated total intensity field in the selected images was adjusted to be the same, and the intensity range was then

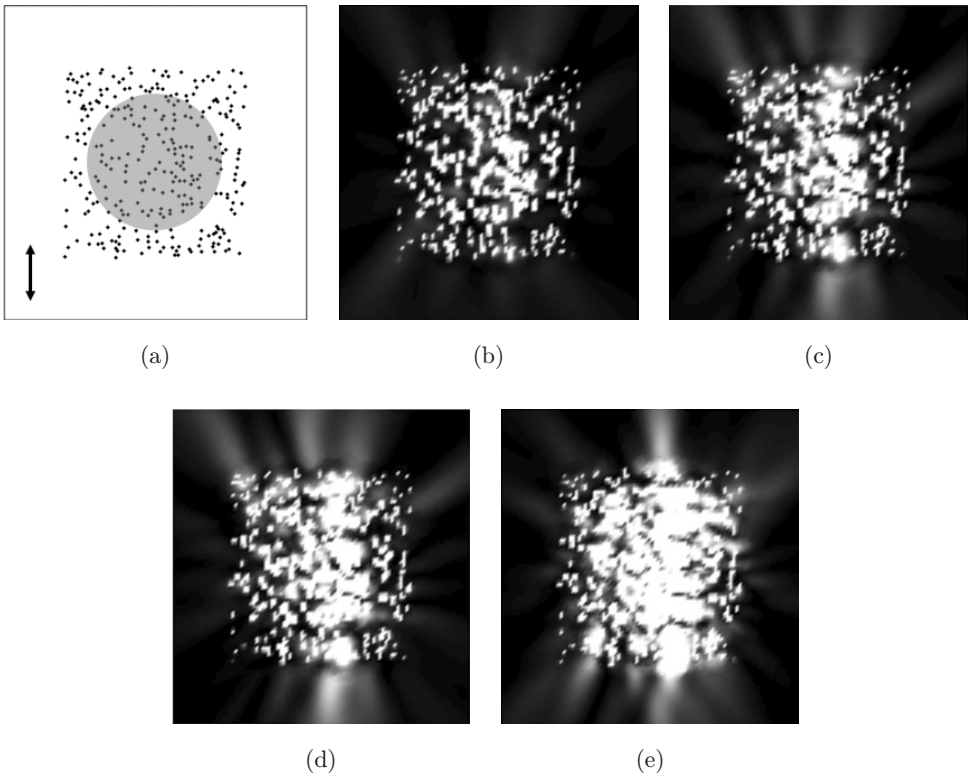

(a) (b) (c)

(d) (e)

Fig. 6. Electric field magnitude distributions ($5 \times 5\,\mu m^2$) for an array of a high number of scatters (a) obtained with the wavelength of (b) 633 nm, (c) 604 nm, (d) 594 nm and (e) 543 nm.

divided by a number of desired intervals from 0 to a maximum intensity $I\max = 1$. Such a procedure allows one for collecting a sufficiently large number (typically, $>10\,000$) of data of the field intensity related to a particular scattering configuration. Having the intensity sampling been determined one can estimate the corresponding PDF. The PDF was approximated by a discrete distribution, whose values were evaluated at the intensity intervals $\Delta I = 0.01$ by counting the number of points n_k with intensities falling in the interval (I_k, I_{k+1}): $\mathrm{PDF}(I_k) = n_k/(N\Delta I)$, where N is the total number of points. The resulted dependencies have been plotted on the logarithmic scale for both the probability and the intensity (Fig. 7). In the regime of well developed multiple SPP scattering the total scattering SPP field becomes dominant, increasing the area with intensities stronger than the incident one. Consequently, one should expect to obtain an asymmetric (positively skewed) PDF.[35,36] The corresponding PDFs for the excitations wavelengths of 633 nm, 612 nm and 604 nm were similar to each other, and followed the form of a positively skewed distribution with a slow exponential decay beyond the maximum probability point (Fig. 7).

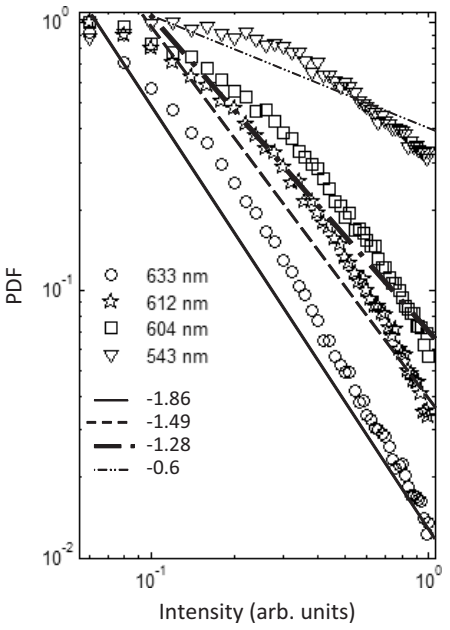

Fig. 7. PDFs based on the simulated images obtained at 633 nm, 612 nm, 604 nm and 543 nm excitation wavelengths for high density of scatterers. The PDF was made by dividing the difference between the maximum and minimum signal from each data set into 100 intervals and counting the number of points having signals within each of these intervals. The straight lines are fitted to the data for each wavelength.

The slopes of the line fits are -1.8 and -1.4 and -1.2 for wavelengths of 633 nm, 612 nm and 604 nm, respectively. These values do follow the power-law dependence as expected with, for instance, fractal clusters of nanoparticles.[37] The PDF obtained for a wavelength excitation of 543 nm exhibited approximately the same amount of larger (constructive interference) and smaller (destructive interference) intensities in the overall total calculated intensity distribution. Apparently, one should expect such a PDF due to the presence of weak multiple scattering[33] derived from the existence of a shorter SPP propagation length.

4. Conclusions

We have developed numerical simulations for elastic SPP scattering in random and periodic nanostructures. We have used the analytic representations of the Green dyadic in the near- and far-field regions, and a suitable limit to distinguish between the uses of these expressions, was presented. We compared the total intensity distributions obtained using the Green dyadic concerned only with the excitation of SPPs to those from a composed Green dyadic for, both, the same nanoparticle configurations and illuminations conditions. Numerical simulations demonstrate practically identical behavior of the total intensities for the case of low density nanoarrays. However, for high density nanoarrays the behavior of the total intensity distributions was different from each other. We conclude that the composed dyadic is a very good choice for the case when the array holds a high density of nanoparticles, since it permits accurate simulations for relatively close nanoparticles. On the reverse, when (on average) the assumption does not hold high density of nanoparticles, the approach using only the Green dyadic for the far-field region resembles good enough observed SPP phenomenon behavior.[3–6] It has also been found that the intensity distributions, exhibiting multiple SPP scattering in high disordered systems and that were calculated by using the composed Green Dyadic, have a similar statistical behavior of predicted experimental and theoretical studies.[38] This issue can be considered as a check to prove the effectiveness of the proposed numerical approach. In order to explore more this approach further theoretical and experimental works are needed for example by using leakage radiation

microscopy.[39] We conduct further research in that direction.

Acknowledgments

Authors acknowledge financial support from CONACyT project SEP-2010-C01-127589 and scholarship 13316.

References

1. H. Raether, *Surface Plasmons*, Springer Tracts in Modern Physics, Vol. 111 (Springer, Berlin, 1988).
2. V. M. Agranovich and D. L. Mills (eds.), *Surface Polaritons* (North-Holland, Amsterdam, 1982).
3. S. I. Bozhevolnyi and V. Coello, *Phys. Rev. B* **58**, 10899 (1998).
4. A. Drezet, A. Hohenau, A. L. Stepanov, H. Ditlbacher, B. Steinberger, F. Aussenegg, A. Leitner and J. Krenn, *Plasmonics* **1**, 141 (2006).
5. I. P. Radko, S. I. Bozhevolnyi, A. B. Evlyukhin and A. Boltasseva, *Opt. Exp.* **15**, 6576 (2007).
6. I. P. Radko, A. B. Evlyukhin, A. Boltasseva and S. I. Bozhevolnyi, *Opt. Exp.* **16**, 3924 (2008).
7. I. I. Smolyaninov, D. L. Mazzoni and C. C. Davis, *Phys. Rev. Lett.* **77**, 3877 (1996).
8. S. I. Bozhevolnyi and F. Pudonin, *Phys. Rev. Lett.* **78**, 2823 (1997).
9. I. I. Smolyaninov, D. L. Mazzoni, J. Mait and C. C. Davis, *Phys. Rev. B* **56**, 1601 (1997).
10. S. I. Bozhevolnyi, J. Erland, K. Leosson, P. M. W. Skovgaard and J. M. Hvam, *Phys. Rev. Lett.* **86**, 3008 (2001).
11. S. I. Bozhevolnyi, V. S. Volkov and K. Leosson, *Phys. Rev. Lett.* **89**, 186801 (2002).
12. Z. Liu, J. M. Steele, W. Srituravanich, Y. Pikus, C. Sun and X. Zhang, *Nano Lett.* **5**, 1726 (2005).
13. A. Drezet, A. L. Stepanov, H. Ditlbacher, A. Hohenau, B. Steinberger, F. R. Aussenegg, A. Leitner and J. R. Krenn, *Appl. Phys. Lett.* **86**, 074104 (2005).
14. D. S. Kim, S. C. Hohng, V. Malyarchuk, Y. C. Yoon, Y. H. Ahn, K. J. Yee, J. W. Park, J. Kim, Q. H. Park and C. Lienau, *Phys. Rev. Lett.* **91**, 143901 (2003).
15. E. Devaux, T. W. Ebbesen, J.-C. Weeber and A. Dereux, *Appl. Phys. Lett.* **83**, 4936 (2003).
16. V. Coello and S. I. Bozhevolnyi, *Opt. Commun.* **282**, 14 (2009).
17. R. Cortes and V. Coello, *Nano* **4**, 201 (2009).
18. A. V. Shchegrov, I. V. Novikov and A. A. Maradudin, *Phys. Rev. Lett.* **78**, 4269 (1997).
19. S. I. Bozhevolnyi and V. S. Volkov, *Opt. Commun.* **198**, 241 (2001).
20. B. J. Soller and D. G. Hall, *JOSA B*, **19**, 2437 (2002).
21. T. Søndergaard and S. I. Bozhevolnyi, *Phys. Rev. B* **67**, 165405 (2003).
22. V. Coello, T. Søndergaard and S. I. Bozhevolnyi, *Opt. Commun.* **240**, 345 (2004).
23. A. B. Evlyukhin and S. I. Bozhevolnyi, *Phys. Rev. B* **71**, 134304 (2005).
24. O. Keller, M. Xiao and S. I. Bozhevolnyi, *Surf. Sci.* **280**, 217 (1993).
25. V. M. Shalaev and S. Kawata (eds.), *Nanophotonics with Surface Plasmons*, Advances in Nano-Optics and Nano-Photonics (Elsevier, The Netherlands 2007),
26. D. P. Tsai, J. Kovacs, Z. Wang, M. Moskovits, V. M. Shalaev, J. S. Suh and R. Botet, *Phys. Rev. Lett.* **72**, 4149 (1994).
27. S. I. Bozhevolnyi, I. I. Smolyaninov and A. V. Zayats, *Phys. Rev. B* **51**, 17916 (1995).
28. P. Zhang, T. L. Haslett, C. Douketis and M. Moskovits, *Phys. Rev. B* **57**, 15513 (1998).
29. V. A. Markel, V. M. Shalaev, P. Zhang, W. Huynh, L. Tay, T. L. Haslett and M. Moskovits, *Phys. Rev. B* **59**, 10903 (1999).
30. S. Grésillon, L. Aigouy, A. C. Boccara, J. C. Rivoal, X. Quelin, C. Desmarest, P. Gadenne, V. A. Shubin, A. K. Sarychev and V. M. Shalaev, *Phys. Rev. Lett.* **82**, 4520 (1999).
31. G. S. Agarwal, *Phys. Rev. A* **11**, 230 (1975).
32. C. Girard, A. Dereux, O. J. F. Martin and M. Devel, *Phys. Rev. B* **55**, 4901 (1997).
33. J. E. Spie, J. F. Young, J. S. Preston and H. M. van Driel, *Phys. Rev. B* **27**, 1141 (1983).
34. V. Coello. *Surf. Rev. Lett.* **15**, 862 (2008).
35. V. Coello and S. I. Bozhevolnyi, *J. Microsc.* **202**, 136 (2001).
36. S. I. Bozhevolnyi and V. Coello, *Phys. Rev. B* **64**, 115414 (2001).
37. M. I. Stockman, L. N. Pandey, L. S. Muratov and T. F. George, *Phys. Rev. Lett.* **72**, 2486 (1994).
38. J. A. Sánchez-Gil and J. V. García-Ramos, *J. Chem. Phys.* **108**, 317 (1998).
39. A. Drezet, A. Hohenau D. Koller, A. Stepanov, H. Ditlbacher, B. Steinberger, F. R. Aussenegg, A. Leitner and J. R. Krenn, *Mater. Sci. Eng. B* **149**, 220 (2008).